Morphosynthesis of Octacalcium Phosphate Hollow Microspheres by Polyelectrolyte-Mediated Crystallization**

Adriana Bigi,* Elisa Boanini, Dominic Walsh, and Stephen Mann

Materials chemists regard the complex processes involved in the formation of biomineralized tissues with increasing interest.[1–5] Indeed, the organic/inorganic composites synthesized by living organisms often display unique and desirable morphological, structural and mechanical properties, and represent informative models for the synthesis and design of complex functional materials.[6, 7] Biomimetic approaches often involve the simulation of one or more of the different strategies used by organisms to selectively control mineral deposition for precise biological requirements.[8] A key principle in biomineralization is the involvement of biological macromolecules, such as phosphoproteins and glycoproteins containing acidic amino acid residues[9] that may be linked into structural organic matrices or secreted as soluble polyelectrolytes within the mineralization environment. When adsorbed onto a substrate, certain proteins extracted from biomineralized tissues can control the nucleation, orientation, polymorphism, and morphology of the mineral phase.[11, 12] This process has prompted a number of analogous studies on mineralization in the presence of synthetic organic templates such as Langmuir monolayers,[13, 14] self-assembled monolayers,[15] functionalized polymer substrates,[5] and supramolecular assemblies.[16] Similarly, because many biomineralization proteins in solution interact with inorganic crystal faces, and thereby inhibit growth and influence the resulting morphology,[10] a wide range of additives, such as small organic molecules,[17, 18] polymers,[19–22] and peptides,[23] have been studied to understand these processes. In the case of certain polymers, complex morphologies that bear little resemblance to the underlying crystal symmetry have been produced.[21, 22] In particular, polyanionic macromolecules such as polyaspartate (PASP) or polyacrylate (PA) have been used to produce elaborate fibrous bundles of barium sulfate,[24] and distorted spirals of calcium carbonate (vaterite).[25]

Herein we show that the crystallization of octacalcium phosphate, $Ca_8H_2(PO_4)_6 \cdot 5H_2O$ (OCP) from aqueous solutions containing PASP or PA at 60 °C and pH 5 results in the direct assembly of a complex inorganic-polymer spherical-shell architecture without the intervention of external templates. The hollow microstructures consist of a thin porous membrane of oriented OCP crystals that are highly interconnected. We show that a hierarchy of processes, involving the radial growth of dense, multilayered spheroids, secondary overgrowth of a porous thin-shell precursor, and anisotropic dissolution of the spheroidal cores, produces this remarkable structure through time-dependent changes in supersaturation and additive concentration.

Synthesis of OCP in the absence of PASP or PA yielded spherulites consisting of long blade-shaped crystals radiating from a common origin (Figure 1). The spherulite diameters

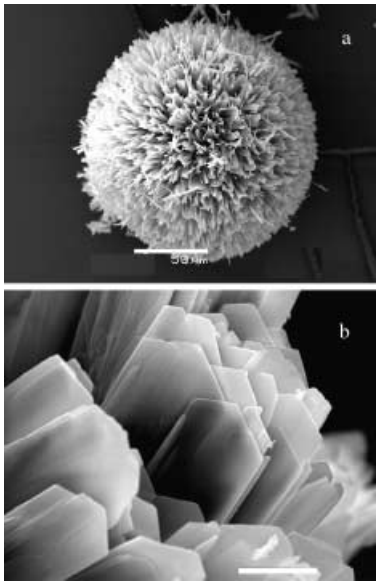

Figure 1. SEM images of a control sample of OCP isolated after 3 h of ageing in the crystallization solution. a) intact spherulite, scale bar: 50 μm, b) higher magnification image showing constituent blade-shaped OCP crystals, scale bar: 5 μm.

ranged between 150–200 μm, and the blades were 2–5 μm wide and 0.3–0.4 μm thick. The platelike morphology is commonly observed for OCP crystals and consists of large basal (100) faces of triclinic pinacoid symmetry that are elongated along the *c* axis and terminated by (011) faces. Addition of PASP or PA to phosphate solutions prior to dropwise addition of calcium acetate resulted in delayed precipitation and the formation of hollow microspheres (referred to as PASP-OCP and PA-OCP, respectively) with diameters up to 1000 μm (Figure 2a,b). The thickness of the shell wall was approximately 10 μm (PASP-OCP) and 20 μm (PA-OCP). Viewed in cross-section, broken fragments showed that the wall was highly porous and consisted of an interconnected network of short platelike OCP crystals (Figure 2c,d). The plates were oriented approximately parallel to the wall thickness such that channel-like pores of about 0.1 to 2 μm traversed the inorganic shell. Furthermore, the lamellar crystals on the surface of the hollow microspheres were slightly shorter and thinner for PASP-OCP than for PA-OCP precipitates (Figure 2e,f), with the consequence that the inorganic membrane produced by the former consisted on average of smaller pores.

X-ray diffraction data indicated that the coherence lengths of crystalline domains were significantly shorter for OCP prepared in the presence of PASP or PA compared with the

[*] Prof. A. Bigi, Dr. E. Boanini
Dipartimento di Chimica "Ciamician"
Universita' degli Studi di Bologna
via Selmi 2, 40126 Bologna (Italy)
Fax: (+39) 051-209-9456
E-mail: bigi@ciam.unibo.it
Dr. D. Walsh, Prof. S. Mann
School of Chemistry, University of Bristol
Bristol BS8 1TS (UK)

[**] This work was supported by MURST, the University of Bologna (Funds for Selected Research Topics), and the EPSRC (UK).

  1433-7851/02/4112-2163 $ 20.00+.50/0

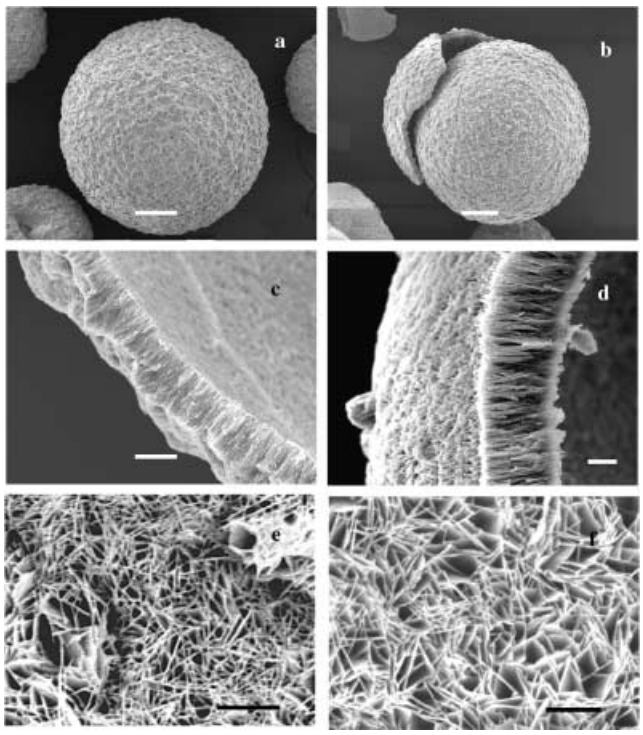

Figure 2. SEM images of OCP microstructures synthesized in the presence of PASP (a, c, e), and PA (b, d, f), and isolated after 3 h of ageing in solution. a, b) Intact hollow shell architectures, scale bars: 100 μm. In (b) a broken fragment of a shell wall is also shown. c, d) Shell-wall cross-sections showing the porous inorganic membrane consisting of an oriented network of OCP crystals, scale bars: 10 μm. e, f) Views of the external surfaces of the hollow spheres showing interconnected network of OCP bladelike crystals, scale bars: 2 μm.

control sample (Table 1). This reduction can be ascribed either to a decrease in crystal perfection because of interactions with the polyelectrolytes, or a result of phase transformation to give small amounts of hydroxyapatite, $Ca_{10}(PO_4)_6(OH)_2$ (HA), or both. Thermogravimetric data indicate that the spherulites contained <1 wt% of the adsorbed polyelectrolytes. Although the amounts were low, even small levels of organic material incorporated into biogenic minerals can greatly affect their structural and mechanical properties.[9] In addition, slight variations in the relative intensity distributions of the X-ray reflections could be attributed to a secondary HA phase, which readily forms by conversion of OCP because of close structural similarity.[26] Accordingly, the Ca:P molar ratio of the solid products increased along the sequence, control OCP, PA-OCP, PASP-OCP (Table 1).

These variations in phase composition are not sufficient however to explain the remarkable morphological differences observed between the polyelectrolyte–OCP microspheres

Table 1. Coherence lengths (τ_{hkl}) evaluated from the width at half-maximum intensity of the 100, 010, and 002 reflections of OCP, OCP-PA, and OCP-PASP materials. The Ca:P molar ratios of the solid products are also reported.

	τ_{100} [nm]	τ_{010} [nm]	τ_{002} [nm]	Ca:P molar ratio
OCP	35 ± 1	45 ± 1	62 ± 4	1.35:1
OCP-PA	22 ± 1	38 ± 1	34 ± 1	1.44:1
OCP-PASP	22 ± 1	24 ± 1	27 ± 1	1.51:1

and the control OCP spherulites. Other investigations were undertaken to determine the stages of growth and assembly of the microstructures by isolating samples from the reaction vessel at different ageing times. In the control experiments, SEM studies of the early stages of growth indicated that the spherulites develop from small, loosely packed aggregates of well-defined blade-shaped crystals that increase in number, length, and particle density as the reaction proceeds (Figure 3). The aggregated morphology of the initial crystals

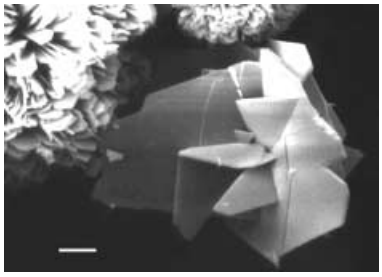

Figure 3. SEM image of early stage in the formation of OCP spherulites grown in the absence of polycarboxylates. The sample was isolated from solution after addition of approximately 50% of the calcium acetate solution to the reaction flask. Scale bar: 10 μm.

probably arises from the high tendency of OCP to undergo multiple twinning, with the wide (100) face acting as twin plane.[26, 27] In contrast, the first OCP-PASP aggregates that could be isolated from solution after complete addition of calcium acetate displayed a compact, spherical morphology (mean diameter = 300 μm), which readily fragmented to reveal cone-shaped domains with remarkable radially banded growth textures (Figure 4 a,b). On further ageing for 1 h in the reaction solution, the layered-growth mechanism was replaced by secondary overgrowth to produce a discrete thin inorganic shell on the surface of the primary spheroids that consisted of short blades oriented perpendicular to the surface

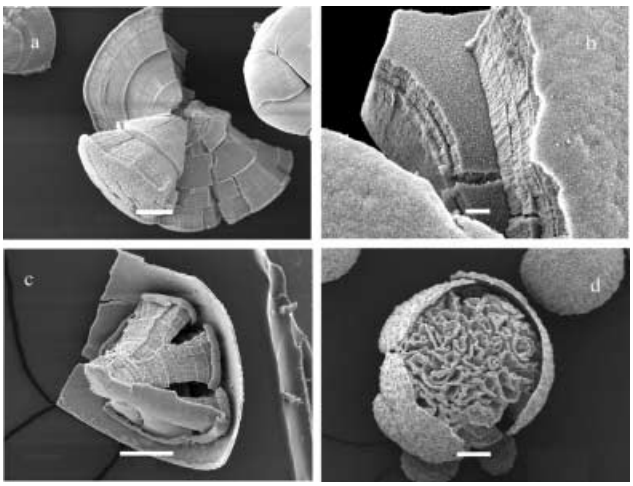

Figure 4. SEM images of OCP-polyelectrolyte architectures synthesized in the presence of PASP and isolated after different periods of ageing in solution: a, b) 45 min, scale bars: 50 μm (a) and 10 μm (b). c) 1 h 45 min, scale bar: 100 μm. d) 3 h, scale bar: 100 μm.

  1433-7851/02/4112-2164 $ 20.00+.50/0

of the core (Figure 4c). Large fragments of the shell membrane were easily detached from the central dense spheroid, indicating that the core–shell interface was discontinuous or only loosely connected. Extending the ageing time resulted in partial dissolution of the banded microstructure to produce a highly porous core with convoluted bicontinuous architecture that was enclosed by the shell wall (Figure 4d). Moreover, dissolution of the spheroids occurred inwardly from the core–shell interface without affecting the texture of the surrounding shell membrane. With time, complete dissolution of the core occurred to give the hollow microspheres shown in Figure 2. Similar results on the growth process were obtained for PA-OCP aggregates.

The spherical morphology and extensive agglomeration of OCP crystals within the layered structure shown in Figures 4a and b can be attributed in part to adsorption of polyaspartate molecules onto the crystal surfaces during growth.[28, 29] Under these conditions, the growth front has to penetrate the polyelectrolyte adsorption layer, with the consequence that the propagation of growth steps across the surface becomes severely hindered and the growth rate decreases. The multilayered banded structure indicates that growth of the spheroidal core is discontinuous with periods of relatively fast growth alternating with periods of stagnation, which presumably take place when the polyelectrolyte concentration on the crystal reaches a critical value, and the distance between the adsorbed molecules becomes smaller than the size of the critical surface nucleus.[28] One possibility is that the delayed onset of nucleation in the presence of the polymers results in the phase separation of highly supersaturated liquid droplets that subsequently undergo polyelectrolyte-mediated crystallization to produce the concentrically layered spheroids. As the process occurs within droplets of confined volume, and involves the 3D radial organization of platelike crystals, significant levels of mechanical stress can build up inside the spheroids. Indeed, the spheroids often underwent catastrophic breakage into cone-shaped fragments when air dried.

Secondary overgrowth of the porous shell on the surface of the spheroids takes place after extensive ageing when the polyelectrolyte concentration in solution is significantly reduced by prior surface adsorption and incorporation within the core microstructure. In the case of PA, which displays a slightly less inhibiting effect on OCP precipitation than PASP, shell formation should start at relatively higher polyelectrolyte concentrations, and result in a thicker shell. Furthermore, the lower levels of polyelectrolyte molecules during growth of the shell produces a more-ordered crystalline phase that is more stable than the multilayered core with respect to dissolution when the solution supersaturation is reduced to close to the solubility limit. Dissolution of the core, initially from the core–shell interface, necessitates diffusion of ions through the shell membrane. The external diameter of the structures did not change appreciably during dissolution, whereas the shell wall increased in size during ageing, as shown for example in Figures 4c and 2c, where the shell wall thickness is approximately 5 μm and 10 μm, respectively. Thus, the dissolution of the core redistributes the mineral ions and contributes to shell-wall growth such that the products isolated after 3 h of ageing consist mostly of hollow microspheres.

In conclusion, polycarboxylates, such as polyaspartate (PASP) and polyacrylate (PA) can be used to synthesize porous hollow microspheres of OCP using a straightforward solution crystallization process. OCP is employed in several technological applications,[30] and is of particular biological importance as a precursor phase in the precipitation of biological apatites.[31] We therefore envisage that the materials reported here will be useful for biomedical applications, such as drug encapsulation and controlled release. Finally, we note that the structural and morphological evolution of inorganic architectures as described here occurs in the absence of external templates through the use of intermediates capable of metamorphism. Such a strategy, involving metastable architectures with hybrid compositions, could have general importance for controlling the synthesis of complex inorganic architectures.

Experimental Section

Synthesis of OCP was carried out by dropwise addition of 0.04 M $Ca(CH_3COO)_2$ (250 mL) over a period of 50 min into a phosphate solution (750 mL) containing Na_2HPO_4 (5 mmol) and NaH_2PO_4 (5 mmol) at a starting pH of 5.[32] The reaction was undertaken at 60 °C with mechanical stirring. The precipitate was left in contact with the mother solution under gentle stirring for different periods of time, up to 3 h. Syntheses in the presence of sodium poly(aspartic acid) ($M_W = 11\,000$) or sodium polyacrylate ($M_W = 2100$) were performed by adding the polyelectrolytes to the phosphate solution. The amounts of polyelectrolytes used were equivalent to a theoretical monomeric unit concentration of 0.044 mM. The resulting OCP precipitates were characterized by scanning electron microscopy (SEM) using a JEOL JSM 5600 LV operating at 12–15 kV. X-ray-diffraction analysis was carried out using a Philips PW 1050/81 powder diffractometer equipped with a graphite monochromator and $Cu_{K\alpha}$ radiation (40 mA, 40 kV). The 2θ range was from 3 to 60° at a scanning speed of 0.5° min^{-1}. Lattice parameters were determined by least-square refinements from the well-determined positions of the most intense reflections. Silicon was used as the internal standard. Differences between the lattice parameters of OCP synthesized in the presence of the polyelectrolytes and those of a control OCP phase, $a = 19.62(5)$, $b = 9.62(9)$, $c = 6.83(6)$ Å, $\alpha = 89.4(8)$, $\beta = 92.6(8)$, $\gamma = 107.4(8)°$, were within the standard deviations. To evaluate the coherence length of the OCP crystals, additional X-ray powder diffraction data were obtained in the relevant region of 2θ by means of step scans using a fixed counting time period of 30 sec and a scan rate of 0.1° $step^{-1}$. The coherence lengths were determined from the width at half-maximum intensity of the 100, 010, and 002 reflections according to the Scherrer equation. The silicon-standard peak 111 was used to evaluate the instrumental broadening. Thermogravimetric analysis was carried out using a Perkin Elmer TGA-7. Heating was performed in a platinum crucible in air flow (20 $cm^3 min^{-1}$) at a rate of 5 °C min^{-1} up to 900 °C. The samples weights were in the range 5–10 mg. Calcium and phosphorus contents of the solid products were determined by means of a Dionex DX100 chromatography system fitted with a Dionex CD20 conductivity detector. The chromatographic data were collected and processed with a Dionex peaknet 5.1 program.

Received: February 4, 2002 [Z 18634]

[1] S. Mann, *Biomineralization. Principles and Concepts in Bioinorganic Materials Chemistry*, Oxford University Press, Oxford, UK, **2001**.
[2] A. A. Campbell, *Curr. Opin. Colloid Interface Sci.* **1999**, *4*, 40–45.
[3] A. H. Heuer, D. J. Fink, V. J. Laraia, J. L. Arias, P. D. Calvert, K. Kendal, G. L. Messing, J. Blackwell, P. C. Rieke, D. H. Thompson,

  1433-7851/02/4112-2165 $ 20.00+.50/0

A. P. Wheeler, A. Veis, A. I. Caplan, *Science* **1992**, *255*, 1098 – 1105.
[4] P. Calvert, P. C. Rieke, *Chem. Mater.* **1996**, *8*, 1715 – 1727.
[5] B. C. Bunker, P. C. Rieke, B. J. Tarasevich, A. A. Campbell, G. E. Fryxell, G. Graff, L. Song, J. Liu, J. Virden, G. Mc Vay, *Science* **1994**, *264*, 48 – 55.
[6] S. Mann, *Angew. Chem.* **2000**, *112*, 3532 – 3548; *Angew. Chem. Int. Ed.* **2000**, *39*, 3392 – 3406.
[7] L. A. Estroff, A. D. Hamilton, *Chem. Mater.* **2001**, *13*, 3227 – 3235.
[8] S. Mann, *J. Chem. Soc. Dalton Trans.* **1997**, 3953 – 3961.
[9] S. Weiner, L., Addadi, *J. Mater. Chem.* **1997**, *7*, 689 – 702.
[10] S. Weiner, L., Addadi, *Trends Biochem. Sci.* **1991**, *16*, 252 – 256.
[11] H. Füredi-Milhofer, J. Moradian-Oldak, S. Weiner, A. Veis, K. P. Mintz, L. Addadi, *Connect. Tissue Res.* **1994**, *30*, 251 – 264.
[12] G. Hunter, *Curr. Opin. Solid State Mater. Sci.* **1996**, *1*, 430 – 434.
[13] S. Mann, B. R. Heywood, S. Rajam, J. D. Birchall, *Nature* **1988**, *334*, 692.
[14] I. Weissbuch, F. Frolow, L. Addadi, M. Lahay, L. Leiserowitz, *Science* **1991**, *253*, 637 – 645.
[15] J. Aizenberg, A. J. Black, G. M. Whitesides, *Nature* **1998**, *394*, 868 – 871.
[16] D. Walsh, J. D. Hopwood, S. Mann, *Science* **1994**, *264*, 1576 – 1578.
[17] P. V. Coveney, R. Davey, J. L. W. Griffin, Y. He, J. D. Hamlin, S. Stackhouse, A. Whiting, *J. Am. Chem. Soc.* **2000**, *122*, 11557 – 11558.
[18] K. Naka, Y. Chujo, *Chem. Mater.* **2001**, *13*, 3245 – 3259.
[19] J. N. Cha, G. D. Stucky, D. E. Morse, T. J. Deming, *Nature* **2000**, *403*, 289 – 292.
[20] S. I. Stupp, P. V. Braun, *Science* **1997**, *277*, 1242 – 1248.
[21] M. Antonietti, M. Breulmann, C. G. Göltner, H. Cölfen, K. K. W. Wong, D. Walsh, S. Mann, *Chem. Eur. J.* **1998**, *4*, 2493 – 2500.
[22] H. Colfen, L. Qi, *Chem. Eur. J.* **2001**, *7*, 106 – 116.
[23] W. Zhang, R. A. Laursen, *FEBS Lett.* **1999**, *455*, 372 – 376.
[24] L. Qi, H. Cölfen, M. Antonietti, M. Li, J. D. Hopwood, A. J. Ashley, S. Mann, *Chem. Eur. J.* **2001**, *7*, 3526 – 3532.
[25] L. A. Gower, D. A. Tirrell, *J. Cryst. Growth* **1998**, *191*, 153.
[26] J. C. Elliott, *Structure and Chemistry of the Apatites and Other Calcium Orthophosphates*, Elsevier, Amsterdam, **1994**.
[27] W. E. Brown, J. P. Smith, J. R. Lehr, A. W. Frazier, *Nature* **1962**, *196*, 1048.
[28] O. Söhnel, J. Garside, *Precipitation: basic principles and industrial applications*, Butterworth-Heinemann, Manchester, **1992**.
[29] G. H. Nancollas, S. J. Zawacki in *Industrial crystallization 84* (Eds.: S. J. Jačić, E. J. de Jong), Elsevier, Amsterdam, **1984**, p. 51.
[30] F. Caruso, *Chem. Eur. J.* **2000**, *6*, 413 – 419.
[31] D. G. A. Nelson, J. C. Barry, *Anat. Rec.* **1989**, *224*, 265 – 276.
[32] R. Z. LeGeros, R.Kijkovska, J. P. LeGeros, *Scanning Electron Microsc.* **1984**, *4*, 1771 – 1777; A. Bigi, E. Boanini, M. Borghi, G. Cojazzi, S. Panzavolta, N. Roveri, *J. Inorg. Biochem.* **1999**, *75*, 145 – 151.

Structural Characterization of a Cationic Zirconocene Olefin Polymerization Catalyst with its Methylated Boralumoxane Counterion**

Bodo Richter, Auke Meetsma, Bart Hessen,* and Jan H. Teuben

The discovery by Sinn and Kaminsky that methyl alumoxane (MAO) can act as an efficient activator for metallocene olefin polymerization catalysts[1] has triggered tremendous developments in single-site olefin polymerization catalysis.[2] Presently, more than twenty years after the initial discovery, the actual nature of MAO and its mechanism of catalyst activation are still under debate.[3] Model studies on *tert*-butyl alumoxanes led Barron et al. to formulate the hypothesis that these alumoxanes consist of oligomeric $(RAlO)_n$ clusters, containing 4-coordinate Al in strained fused 4-membered Al_2O_2 rings that can exhibit "latent Lewis acidity" by ring opening, allowing Al to abstract an alkyl anion from the transition metal dialkyl catalyst precursor.[4, 5] The direct (structural, spectroscopic) study of these processes and their products is hampered by the apparent equilibrium nature of the alkyl transfer reaction, with the equilibrium constant strongly favoring the starting materials when well-defined alumoxanes with sterically demanding alkyl groups are used. Crystal structure determinations of the products resulting from the reaction of $[t\mathrm{BuAlO}]_6$ with MeLi[5] and with RNH_2[6] gave support for the proposed activation mechanism, but as yet the products of the activation of metallocene single-site olefin polymerization catalysts by alumoxane activators have eluded full characterization.

Recently we reported the synthesis and structural characterization of a well-defined boralumoxane species, $[t\mathrm{Bu}_4\mathrm{Al}_4\mathrm{Ar}_4\mathrm{B}_4\mathrm{O}_8]$ (**1**, Ar = 2,6-diisopropylphenyl), and showed that this compound is able to activate $[\mathrm{Cp}_2\mathrm{ZrMe}_2]$ for catalytic ethene polymerization.[7] Although **1** is topologically quite

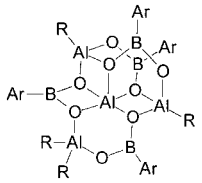

1 (R = *t*Bu, Ar = 2,6-*i*Pr$_2$C$_6$H$_3$)

different from the *t*Bu-alumoxane species isolated by Barron et al., containing 3-coordinate B and 4- and 5-coordinate Al, it shares with these compounds the presence of a strained 4-membered Al_2O_2-ring assembly (edge sharing with a $BAlO_2$

[*] Dr. B. Hessen, Dr. B. Richter, A. Meetsma, Prof. Dr. J. H. Teuben
Dutch Polymer Institute/Center for Catalytic Olefin Polymerization
Stratingh Institute for Chemistry and Chemical Engineering
University of Groningen
Nijenborgh 4, 9747 AG Groningen (The Netherlands)
Fax: (+31) 50-3634315
E-mail: hessen@chem.rug.nl

[**] Netherlands Institute for Catalysis Research (NIOK) publication RUG 02-04-01.

Supporting information for this article is available on the WWW under http://www.angewandte.org or from the author.

  1433-7851/02/4112-2166 $ 20.00+.50/0